

# RSC Advances



This is an *Accepted Manuscript*, which has been through the Royal Society of Chemistry peer review process and has been accepted for publication.

*Accepted Manuscripts* are published online shortly after acceptance, before technical editing, formatting and proof reading. Using this free service, authors can make their results available to the community, in citable form, before we publish the edited article. This *Accepted Manuscript* will be replaced by the edited, formatted and paginated article as soon as this is available.

You can find more information about *Accepted Manuscripts* in the [Information for Authors](#).

Please note that technical editing may introduce minor changes to the text and/or graphics, which may alter content. The journal's standard [Terms & Conditions](#) and the [Ethical guidelines](#) still apply. In no event shall the Royal Society of Chemistry be held responsible for any errors or omissions in this *Accepted Manuscript* or any consequences arising from the use of any information it contains.

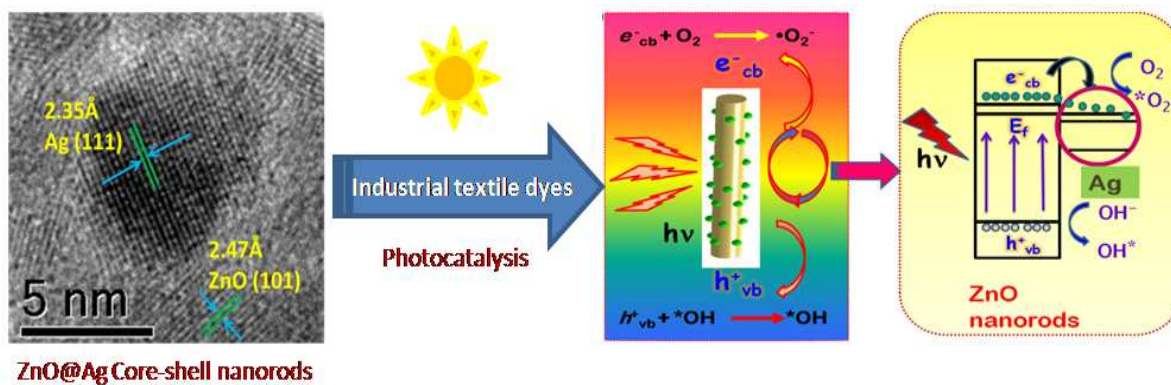
## TOC Graphics

# Plasmon -Mediated Highly Enhanced Photocatalytic Degradation of Industrial Textile Effluent Dyes using Hybrid ZnO@Ag Core-shell Nanorods

V.P.Dinesh<sup>a</sup>, P.Biji<sup>a\*</sup>, Anuradha Ashok<sup>a</sup>, S.K.Dhara<sup>b</sup>, M.Kamaruddin<sup>b</sup>, A.K.Tyagi<sup>b</sup> and Baldev Raj<sup>a</sup>

<sup>†</sup> Nanotech Research Facility, PSG Institute of Advanced Studies, Coimbatore - 641 004, INDIA

<sup>‡</sup> Indira Gandhi Center for Atomic Research, Kalpakkam- 603102, INDIA.



Cite this: DOI: 10.1039/c0xx00000x

www.rsc.org/xxxxxx

ARTICLE TYPE

## Plasmon –Mediated, Highly Enhanced Photocatalytic Degradation of Industrial Textile Dyes using Hybrid ZnO@Ag Core-shell Nanorods

V.P.Dinesh<sup>a</sup>, P.Biji<sup>a\*</sup>, Anuradha Ashok<sup>a</sup>, S.K.Dhara<sup>b</sup>, M.Kamaruddin<sup>b</sup>, A.K.Tyagi<sup>b</sup> and Baldev Raj<sup>a</sup>*Received (in XXX, XXX) Xth XXXXXXXXX 20XX, Accepted Xth XXXXXXXXX 20XX*

DOI: 10.1039/b000000x

### ABSTRACT

Hybrid ZnO@Ag core-shell heterojunction nanorods were synthesized using a novel, facile two-step process based on hydrothermal and seed mediated growth techniques. The material was characterized by UV-visible spectroscopy, Fourier transform - infra red spectroscopy (FT-IR), room temperature photoluminescence spectroscopy (RTPL), Raman spectroscopy, Thermo gravimetric analysis (TGA), X-ray diffraction (XRD), High resolution transmission electron microscopy (HRTEM) and X-ray photoelectron spectroscopy (XPS). The hybrid ZnO@Ag core-shell nanorods were comprised of one dimensional (1D) ZnO nanorods serving as a core material over which surface-doped Ag nanoclusters (~2.5 nm) anchored as a heterogeneous shell. Presence of oxygen vacancies and Zn interstitials were confirmed by RTPL and Raman spectroscopic analysis. The photocatalytic activity of the hybrid ZnO@Ag core-shell nanorods was studied in comparison to bare ZnO nanorods using standard R6G dye and industrial textile dyes, such as, Congo Red and Amido black10B under UV and visible light (solar) irradiations. Moreover, the material was tested for real time industrial textile effluents under ambient conditions and was found to be highly efficient. The enhanced photocatalytic property observed for ZnO@Ag hybrid core-shell nanorods is attributed to phenomenal increase in oxygen related defects in the core that generate photo-induced charge carriers and presence of plasmonic Ag nanoclusters in shell which act as a sink for the photo-induced charge carriers.

### INTRODUCTION

The residual dyes from textile and various industries are considered as the major constituents of organic pollutants when introduced to natural water resources causing severe environmental pollution. About 2-20% of the dyes used in dyeing process is released as textile effluents.<sup>1</sup> These colored organic dyes provoke serious environmental hazards by engendering water pollution and eutrophication to aquatic lives and can stimulate perilous products through chemical reactions.<sup>2</sup> Hence, degradation of organic pollutants, such as, textile dyes has received a lot of attention leading to environmental remedial process. There are lots of non-destructive physical processes used for the degradation of textile and industrial dyes, but they just transfer the organic compounds into another phase causing secondary pollutants.<sup>3</sup> Similarly, biological and chemical methods are performed at dawdling phase with high operating cost.<sup>4</sup> Current practices and technologies being inadequate; the need for eco- friendly\_and cost effective remedies has paved the way for the emergence of a new destructive technique, known as advanced oxidation process (AOPs). In this process, very reactive species like hydroxyl radicals (OH<sup>•</sup>) oxidize a wide range of organic pollutants rapidly and randomly leading to complete

mineralization of organic dyes into CO<sub>2</sub>. AOPs have been used by varied processes starting from Fenton, photo-Fenton catalytic reactions, UV-H<sub>2</sub>O<sub>2</sub> processes, and TiO<sub>2</sub> mediated photocatalysis.<sup>5</sup> Among various materials used for AOPs, semiconducting metal oxide materials are inexpensive, non toxic and possess high chemical stability. Metal oxide semiconductors (MOS), such as, ZnO and TiO<sub>2</sub> having wide band gaps have widely been used as photocatalysts owing to their high catalytic property and environmental sustainability.<sup>6,7</sup> However, it is found that photocatalytic efficiency of MOS is affected greatly due to the recombination (upto 90%) of photogenerated charge carriers.<sup>8</sup> Whereas, nanosized MOS (both 0D and 1D) has more advantage over their bulk due to their increased surface-to-volume ratio, size comparable to the Debye screening length, more active sites and reduced recombination process.<sup>9</sup> Though zero-dimensional (0D) TiO<sub>2</sub> and ZnO nanoparticles exhibit enhanced photocatalytic properties as compared to their bulk counterpart, to retrieve these fine powdered photocatalysts from the photocatalytically treated water is very difficult affecting the reutilization process.<sup>10</sup> Apart from this, aggregation of 0D nanoparticles occurs in solution state which drastically affects the efficiency by inhibiting the formation of hydroxyl radicals. To overcome these hindrances, 1D nanomaterials are the most suited candidates as they are

highly stable against aggregation and also ease in recovery process after photocatalysis. Apart from this, 1D nanostructure has faster electron diffusion process than 0D particles due to the formation of a space charge layer which acts as an energetic barrier in recombination process.<sup>11</sup>

Photocatalytic efficiency of MOS can be further increased significantly by introducing metal/semiconductor heterojunctions since noble metals (Au, Ag and Pt) can act as reservoirs for photo-generated electrons; thereby supporting interfacial charge separation processes.<sup>12,13</sup> Synthesis of hybrid 1D semiconductors having heterojunctions is a challenging process and has been done using a number of chemical methods such as co-precipitation, chemical vapour deposition, hydrothermal deposition – precipitation.<sup>14,15</sup> But some of the important issues still persists and are yet to be addressed during the formation of hybrid nanostructures. Uniform deposition of metal nanoparticles with controlled size over the semiconductors is one of the key issues in research. So far, TiO<sub>2</sub> based hybrid nanoparticles were extensively used as photocatalysts whereas, ZnO based hybrid nanostructures were not much exploited. It is to be mentioned that, ZnO can be tailor made into any nanostructure and dimensions as per our applications, adopting simple synthetic routes. Moreover, ZnO can also be used as a feasible alternative to TiO<sub>2</sub> with a wide band gap of 3.37 eV, very large exciton energy of 60 meV, and an electron affinity of 4.2 eV, making it as a promising material for a variety of applications.<sup>16</sup> Among noble metal catalysts, Ag doped MOS has shown promising efficiency for varied applications because of its unique plasmonic properties and antimicrobial effects.<sup>17</sup> Recently, scientists have reported that Ag doped heterojunction nanoparticles show an enhanced photocatalysis with increased efficiency due to photoinduced electron transfer process upon UV irradiation.<sup>18</sup> Therefore, for this investigation, Ag was chosen to form heterojunctions on the surface of 1D ZnO nanorods forming ZnO@Ag core-shell nanorods. Though there are lots of approaches for the synthesis of Ag/ZnO based heterostructures using wet chemical and hydrothermal routes,<sup>19</sup> the major difficulty observed in these methods is that Ag nanoparticles tend to form aggregates rather than nanoclusters. The aggregation of Ag nanoparticles will directly affect the efficiency of photocatalysis and photoelectric properties, because of the decreased contact between Ag and ZnO interfaces. As a result the rational synthesis of ZnO@Ag core-shell nanorods with specific 1D morphology and well defined interface directly plays a significant role in the charge transport properties. Thus, it is essential to develop simple and efficient methods for the controlled deposition of Ag nanoclusters onto the surface of 1D MOS. Deposition of Ag nanoclusters onto 1D SMOs plays an important role in charge distribution and consequently influences the optical and photocatalytic properties. Herein, we report a novel, facile two-step process for the synthesis of hybrid ZnO@Ag core-shell hetero-junction nanorods at room temperature with Ag nanoclusters surface decorated over the ZnO nanorods. Though several precipitation and reduction methods were reported for the synthesis of core-shell heterojunctions, we have adopted simple seed mediated growth method using Triethylamine (TEA) as reducing agent. Slow reduction process using a weak reducing agent, TEA was found to be highly efficient in controlling the nanocluster formation

during seed mediated growth, compared to previous reports. Well defined interfaces between ZnO and Ag and a favoured crystallographic relationship between metal nanoparticles and MOS have been identified additionally. According to many reports, some external factors like heat treatment are required to enhance photocatalysis process.<sup>20,21</sup> But, for the method reported in this work, no such treatment is required. Hybrid ZnO@Ag core-shell nanorods produced using this synthetic strategy was found to exhibit excellent photocatalytic properties towards degradation of R6G, Congo Red and Amino Black dyes owing to the plasmonic effects of Ag nanoclusters on the ZnO nanorod surface. Interestingly, the material was showing good degradation efficiency for real time industrial textile effluents also under both UV and solar irradiations. The active role of plasmonic Ag nanoclusters on ZnO nanorods during photocatalysis and probable mechanism is discussed and proposed. The synthetic strategy revealed in this study followed by its photocatalytic applications paves a way for realistic solution needed in textile industries.

## EXPERIMENTAL SECTION

### Materials and Methods

Zinc chloride (98%, Merck), Potassium hydroxide (98%, Merck), Silver nitrate (99.9%, Merck), Cetyl trimethylammonium bromide (CTAB) (99%, Merck), Ethanol (99%, Merck), Triethylamine (TEA) (99% Merck) and 3-aminopropyl-trimethoxysilane (APTMS) (99%, Aldrich) were taken as precursors. All chemicals were used as such without any further purification. Ultrapure water with a resistivity of 18.2 MΩ.cm was used (Millipore Milli-Q system) for the synthesis.

**Synthesis of ZnO nanorods.** The ZnO nanorods used in this study was prepared according to previously reported procedure.<sup>22</sup> In brief, 10 mL of 2 mM KOH solution was added dropwise into the 20 mL of 1 mM ZnCl<sub>2</sub> solution and stirred vigorously. 5mL of 0.5 mM CTAB solution was added to the stirring solution and white floccules appear immediately indicating the formation of zinc hydroxide. After 3 hours of continued stirring, the solution was transferred into a Teflon-lined stainless steel autoclave and filled by distilled water up to 80% volume. Hydrothermal treatments were carried out at 120°C for 5 h. After this process, autoclave was allowed to cool down naturally and white precipitates of ZnO nanorods were separated via centrifugation, washed thoroughly using distilled water and ethanol to remove impurities. Finally, the ZnO nanorods were dried at 80°C in hot air oven for 8 h.

**Synthesis of Hybrid ZnO@Ag core-shell nanorods.** In order to functionalize the ZnO nanorods, 2 mg of the ZnO nanorods were weighed and dispersed in 10 mL of 1M ethanol. 50 μL of 1M 3-aminopropyl-trimethoxysilane (APTMS) was added to the dispersion and stirred for 12 h continuously. After completion of functionalization reaction, the precipitate was separated and washed several times using distilled water and ethanol, and further dried at 60°C. 10 mL of 7.5 M triethyl amine (TEA) solution was taken in a round bottom flask and 2 mg of APTMS functionalized ZnO nanorods were added and stirred for 30

Cite this: DOI: 10.1039/c0xx00000x

www.rsc.org/xxxxxx

ARTICLE TYPE

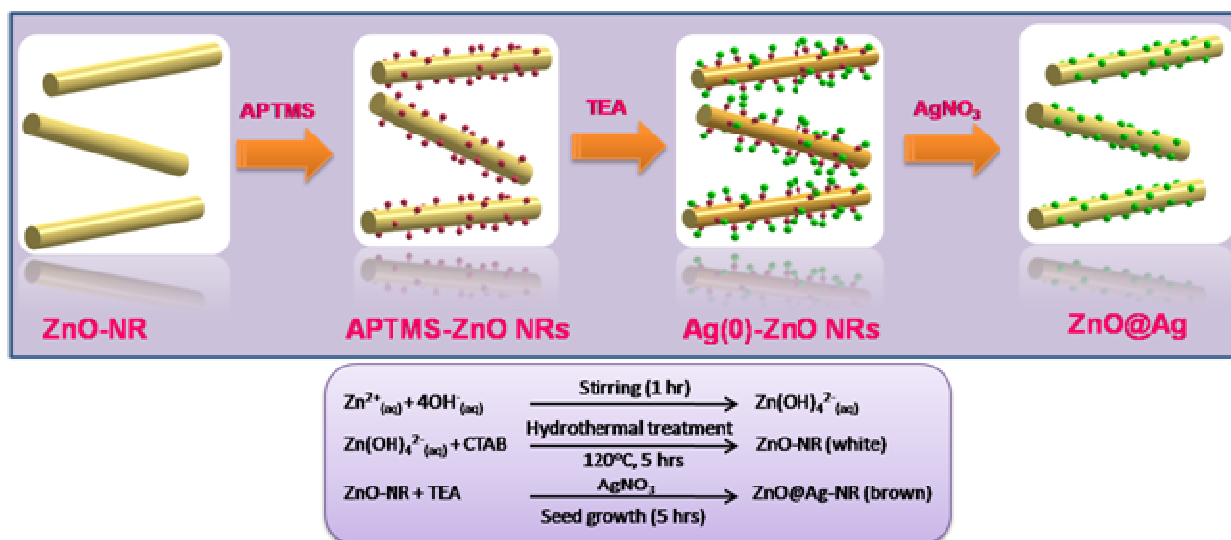


Fig.1. Schematics of the synthetic process adopted for the growth of hybrid ZnO@Ag nanorods.

minutes. 2 mL of 0.6 M of  $\text{AgNO}_3$  solution was added dropwise to the mixture. A dark brown precipitate was formed immediately after the addition indicating the formation of ZnO@Ag core-shell nanorods. 100 mL of distilled water was added to the dark brown precipitate and solution was left undisturbed for 5 hours for seed growth. The precipitate was separated and purified carefully using distilled water and ethanol several times using centrifuge and vacuum filtration to remove impurities. Further, the materials were air dried overnight at  $80^\circ\text{C}$ . The purified hybrid ZnO@Ag core-shell nanorods were further used for photocatalytic degradation of R6G and industrial textile dyes.

#### Characterization Techniques.

The purified ZnO@Ag nanorods were well characterized spectroscopically and microscopically. UV-vis absorption spectra were acquired using T90+UV-Visible spectrophotometer (PG Instruments, UK). The FT-IR analysis was done using Nicolet Impact 400 FT-IR spectrophotometer using KBr pellets. Micro Raman and PL studies were conducted using a He-Cd laser as the excitation light source at 325nm with 2400g/mm gratings in the backscattering configuration of a spectrometer (inVia Renishaw, UK). Thermo gravimetric analysis was completed using Perkin Elmer STA 600 instruments with a scanning rate of  $10^\circ$  per min. Powder XRD patterns were taken for all the calcined samples using XRD power X-ray diffractometer (JSO-DEBYEFLEX 2002) using Cu K $\alpha$  radiation of wavelength 1.54 nm with a scanning rate of  $0.02^\circ/\text{sec}$  in the  $2\theta$  range of  $10-70^\circ$ . The structure and morphology of the hybrid core-shell nanomaterials were examined using High-Resolution Transmission Electron Microscopy (JEOL JEM-2010, Japan) and Field Emission Scanning Electron Microscope (ZEISS SUPRA 55) in-build with

an energy-dispersive X-ray spectrometer (Oxford Instruments, INCA, UK). X-ray photoelectron spectroscopy (Omicron Nanotechnology, Germany) was used to analyze structural composition of the ZnO@Ag hybrid nanostructures.

#### Photocatalytic dye degradation studies.

Photocatalytic properties of the hybrid ZnO@Ag core-shell nanorods were evaluated by observing the catalytic degradation of Rhodamine 6G standard dye. The photocatalytic experiments were performed under atmospheric conditions. Aqueous solution of R6G dye was treated with hybrid ZnO@Ag core-shell nanorods just before the experiment and purged with Nitrogen to remove dissolved oxygen. The concentration of the catalyst in the reaction mixture was optimized as 25 mg/L against the dye concentration of 10 ppm. The catalyst suspension was mixed thoroughly using ultrasonication (15 min) to attain equilibrium adsorption on the catalyst surface. Photocatalysis was performed with the UV radiation from fluorescent Hg lamp (Philips TUV 4W: the strongest emission around  $\lambda = 360$  nm). Under similar conditions, experiments were also carried using full spectrum Solar Simulator using Abet 10500 Class A Solar Simulator fitted with Xenon arc lamp (AM = 1.5G). The photocatalytic degradation was monitored using UV-Vis Spectroscopy by measuring the absorption of R6G at 525 nm as a function of irradiation time. All the absorbance values were averaged out of three independent measurements. Similar experiments were conducted using industrial textile dyes such as Congo red, Amido Black to establish the dye degradation efficiency using the ZnO@Ag core-shell nanorods. Industrial textile effluents used for real sample testing were collected from a textile industry located in Thirupur, India.

Cite this: DOI: 10.1039/c0xx00000x

www.rsc.org/xxxxxx

## ARTICLE TYPE

## RESULTS AND DISCUSSION

Hybrid core-shell nanorods were prepared via a combination of hydrothermal method and *in-situ* reduction method using bifunctional ligands. Hydrothermally synthesized ZnO nanorods were used as the core, which were further functionalized using APTMS ligands. The APTMS functionalized ZnO nanorods were then treated with AgNO<sub>3</sub> and *in-situ* reduced using TEA and a dark brown precipitate of hybrid ZnO@Ag core-shell nanorods was obtained. Figure 1 represents the schematic representation of hybrid core-shell nanorods formation.

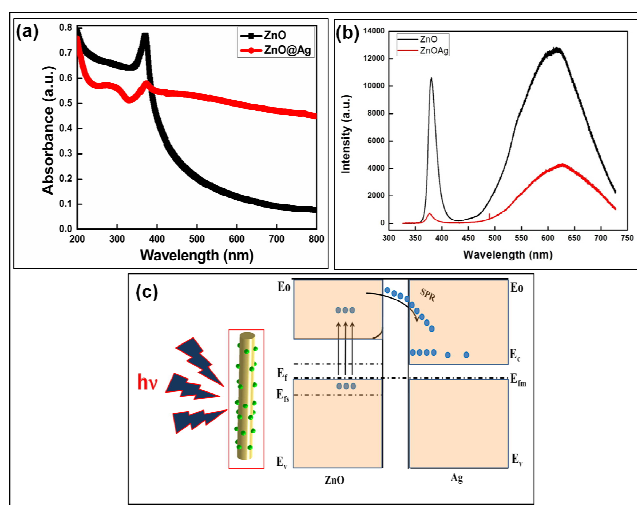


**Fig. 2.** (a) UV – Visible spectra of ZnO nanorods and hybrid ZnO@Ag core-shell nanorods, (b) PL spectrum of ZnO nanorods and hybrid ZnO@Ag core-shell nanorods and (c) The energy band structure of hybrid ZnO@Ag core-shell nanorods.

UV-Visible absorbance spectra of ZnO nanorods and ZnO@Ag hybrid nanorods were shown in the Figure 2a. The characteristic peak appearing at 370 nm corresponds to the ground excitonic peak of pure ZnO nanorods.<sup>23</sup> Absence of additional adsorption peaks in the UV-Visible spectrum further confirms the purity of the ZnO nanorods. In hybrid ZnO@Ag core-shell nanorods, a red shifted peak at 373 nm was observed due to the strong interfacial electronic coupling between ZnO and Ag atoms.<sup>24</sup> In the heterostructures, electron transfer process happens from ZnO and Ag owing to divergence in the fermi levels.<sup>24</sup> A sharp peak centered at 270 nm is observed for hybrid ZnO@Ag core-shell nanorods which reveals the presence of silver nanoclusters having diameter less than 5 nm.<sup>25</sup> Here, TEA was used to reduce the Ag<sup>+</sup> ions to form Ag<sup>0</sup> which is a weak reducing agent compared to sodium borohydride.<sup>26</sup> The *in-situ* reduction of Ag<sup>+</sup> leads to the formation of Ag nanoclusters on the surface of ZnO nanorods. The so-formed Ag<sup>0</sup> atomic clusters creates nucleation centers on the surface of APTMS functionalized ZnO nanorods for further growth as nanoclusters. The domination of Ag nanoclusters over

Ag nanoparticles gives rise to an inconspicuous shoulder peak at 270 nm, decreasing its plasmon peak to 420 nm. Also, the exciton peak of ZnO at 373 nm dominates over the plasmon peak of Ag nanoparticles. This is attributed to defects being utilized for Ag nanoclusters growth over the ZnO nanorods.<sup>27</sup> Similar effect was observed in Au nanoclusters in the previous reports where, the surface plasmon absorbance decreases as a function of reduction in cluster size.<sup>28</sup> Thus, optical absorbance studies reveals the formation of Ag nanoclusters on the surface of ZnO nanorods which was further confirmed from HR-TEM analysis. Photoluminescence studies gave an insight into the optical and photochemical properties of the hybrid ZnO@Ag core-shell nanorods. PL spectra revealed the structural defects such as, oxygen vacancies, zinc interstitials etc., the charge distribution and Fermi level equilibrium in ZnO@Ag heterostructures. The room temperature PL spectra (excitation at 325 nm) for ZnO and hybrid ZnO@Ag nanorods are depicted in Figure 2b. A strong excitation peak shows a UV emission band centered at 380 nm corresponding to the near band edge emission of ZnO nanorods due to excitonic recombination through an exciton-exciton collision process and reflects the high crystalline nature of the ZnO nanorods.<sup>29</sup> High intensity peak observed at the yellow orange region and green emission regions (Fig.2b) are due to the presence of oxygen related defects and interstitials present in ZnO nanorods.<sup>30,31</sup> The PL intensity of hybrid ZnO@Ag core-shell nanorods appears lower when compared to ZnO nanorods. This is attributed to the formation of Ag nanoclusters over ZnO nanorods which accept electrons and leads to the increased charge separation effects for photo-induced electrons-holes pairs. As the Ag nano-clusters start growing over the ZnO nanorods, primarily the decline of crystal defects occurs leading to the relaxed nature of charge carriers via surface related traps and thereby quenching the emission peak of ZnO. This process influences the charge carrier dynamics of the hybrid materials.<sup>31,32</sup> The decrease in emission intensity is in accordance with the Stern-Volmer quenching effect reported in literatures.<sup>33</sup> Variation of V<sub>o</sub>'' defect density on the surface of ZnO nanorods is related to the high surface-to-volume ratio and the interfaces between Ag nanoclusters and ZnO nanorods.<sup>20</sup> Upon irradiation of incident light with wavelength larger than particle size, high-density electron cloud of noble metal nanoclusters forms and tends to oscillate. In the hybrid materials, electrons accumulate at the metal-semiconductor junctions leading to upward band bending for ZnO and thus favoring straightforward transfer of electron from ZnO to Ag nanoclusters, which prevents the charge carrier recombination process<sup>34</sup> as depicted in Figure 2c. From the PL studies Ag nanoclusters on the ZnO surface block both direct trap related charge carrier recombination pathways by extracting electrons from the photoinduced ZnO.<sup>18</sup> Thus, a majority of the extracted electrons are utilized for the catalytic degradation process leading to enhanced photocatalytic activity.

Cite this: DOI: 10.1039/c0xx00000x

www.rsc.org/xxxxxx

ARTICLE TYPE

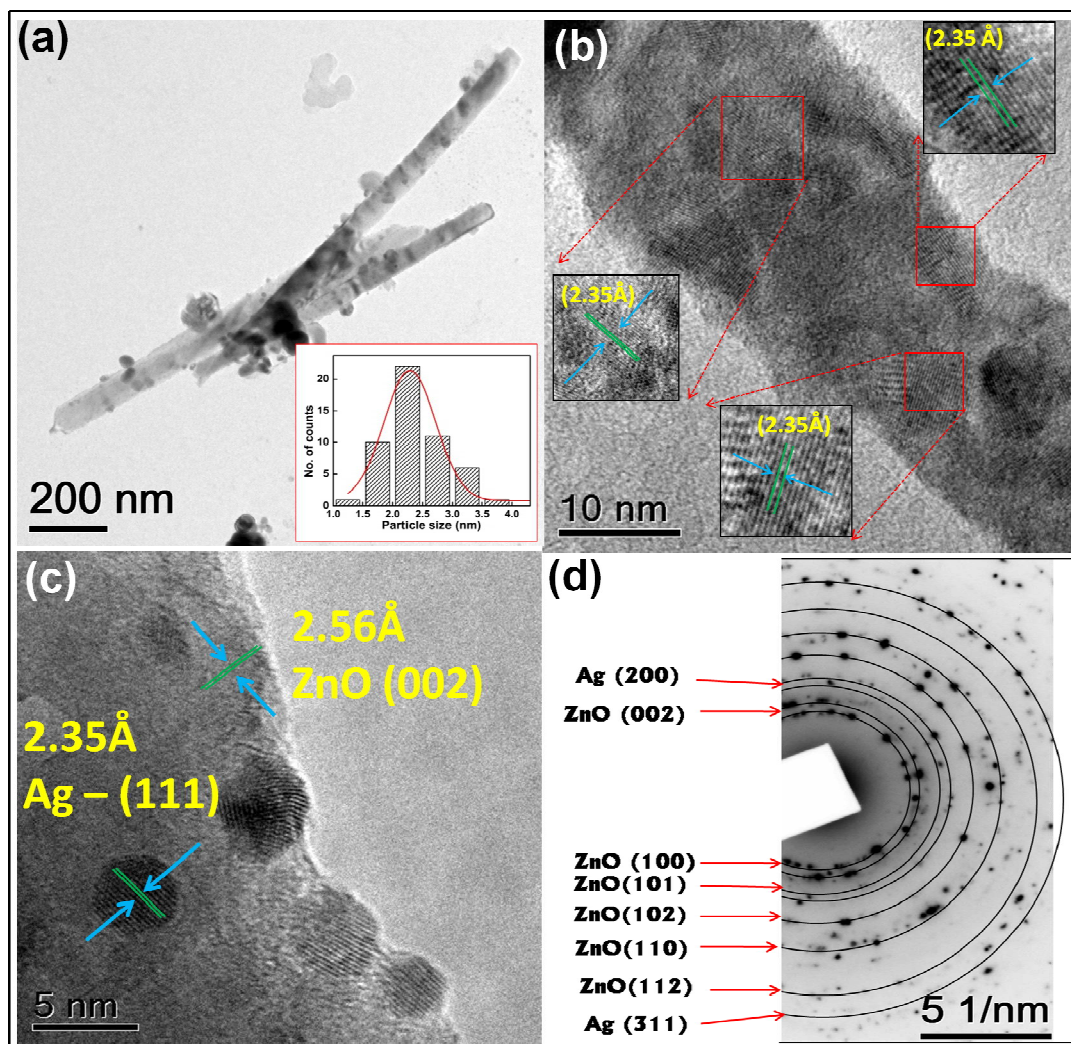


**Fig.3.** (a) Representative TEM images of hybrid ZnO@Ag core-shell nanorods, high resolution TEM images showing (b) the Ag nanoclusters decorated over ZnO nanorods, (c) surface doped Ag nanoclusters and (d) SAED pattern analysis of hybrid ZnO@Ag core-shell nanorods.

Morphological and structural analysis of the core-shell ZnO@Ag nanorods were further carried out using FE-SEM, X-ray diffraction studies and Raman Spectral analysis. FE-SEM studies of hybrid core-shell nanorods showed the monodispersed nanorods and EDS showed the loading percentage of Ag onto ZnO nanorods of 6.90% (See Figure S1, Supporting Information). XRD studies of ZnO nanorods showed their characteristic peaks with hexagonal wurtzite structure with space group of  $P6_3mc$ . XRD data of hybrid ZnO@Ag core-shell nanorods reveals peaks corresponding to Ag along with those of ZnO confirming the formation of hybrid structures (See Figure S2 and Table S1, Supporting Information). Raman spectroscopy is another powerful technique used to infer about the optical phonon modes, phase purity and vibrational properties of ZnO nanorods and ZnO@Ag hybrid core-shell nanorods. ZnO nanorods show two

asymmetric longitudinal optical multi-phonon peaks at 579 and 1150  $\text{cm}^{-1}$ , whereas hybrid ZnO@Ag core-shell nanorods shows red shift for LO phonon modes with appreciable peak broadening effect due to the growth of Ag nanoclusters onto the ZnO nanorods (See Figure S3, Supporting Information). FE-SEM and TEM images of bare ZnO nanorods synthesised by hydrothermal method are shown in Figure 4(a,b). As evident from the microscopic images ZnO nanorods of uniform length and width were obtained using the hydrothermal synthesis. Similarly, TEM analysis (Figure 4b) divulges well defined boundaries of nanorods. Selected area diffraction (SAD) studies reveals the nanorods were grown from (100), (110) and (112) planes and this matches well with the XRD studies (S2) of hexagonal wurtzite structured ZnO (JCPDS PDF no 36-1451).

TEM analysis was carried out to infer about the structure and

morphology of the hybrid ZnO@Ag core-shell nanorods. As evident from Figure 3, the HRTEM image clearly shows the uniform distribution of Ag nanoclusters on the surface of ZnO nanorods and confirms the formation of hybrid nanostructures with core-shell hetero-junctions. Ag nanoclusters anchored onto the ZnO nanorods shows an average particle size of  $\sim 2.5$  nm (inset, Figure 3a) and no aggregation was observed during the binding process, providing an effective synthetic process. The HRTEM image analysis (Figure 3b,c) shows the notable interface structures with continuity of lattice fringes between the Ag nanoparticles and ZnO nanorods that confirms the chemical bonding between two particles. For ZnO nanorods the adjacent lattice fringes space was calculated as 0.256 nm which matches with the  $d$  spacing of the (002) plane of hexagonal structure and hence confirms the single crystalline structure of ZnO nanorods with a preferred growth direction of [001]  $c$  axis.<sup>34-37</sup> Whereas, for Ag nanoclusters the distance between adjacent lattice fringes was calculated as 0.235 nm, close to the  $d$ -spacing value of (111) plane of *fcc* Ag. These values confirm that the [110] direction ( $c$  axis) is the preferred growth direction of Ag nanoclusters which matches with the XRD data. It is further confirmed by the HRTEM analysis (Figure 3c) showing the zone axis of *fcc* Ag along [110] zone. Growth of Ag nanoclusters onto the ZnO nanorods occurs due to the lattice mismatch of Ag and ZnO.<sup>35</sup> Similarly, SAED pattern (Figure 3d) shows prominent ring patterns corresponding to ZnO and Ag. These mixed diffraction patterns confirm the presence of Ag nucleus on the interfacial ZnO nanorods. This confirms the structure of ZnO@Ag core-shell nanorods during seed mediated process using APTMS, which act as an active site for the growth of nanoclusters. The free amino group of APTMS can easily form a complex with Ag(I) creating active sites for silver cluster growth which can also enhance the anchorage of Ag nanoclusters.<sup>38</sup> The resulting Ag (I)-amino-silanols complexes were reduced by TEA to form ZnO@Ag core-shell nanorods (Figure 1).

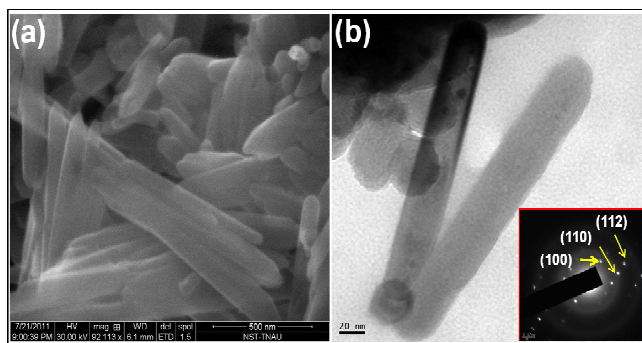


Fig. 4. (a) FE-SEM image and (b) TEM image of bare ZnO nanorods (inset shows the SAD pattern of ZnO).

XPS analysis was performed to corroborate the elemental and chemical states to elucidate the structure of hybrid ZnO@Ag core-shell nanorods and its corresponding spectra were depicted in the Figure 5. The binding energies observed in the XPS spectra are calibrated using C 1s (284.8 eV). All peaks in the Figure 4a are ascribed to Zn, Ag, O and C elements and no other peaks are observed, confirming the sample composes of three elements

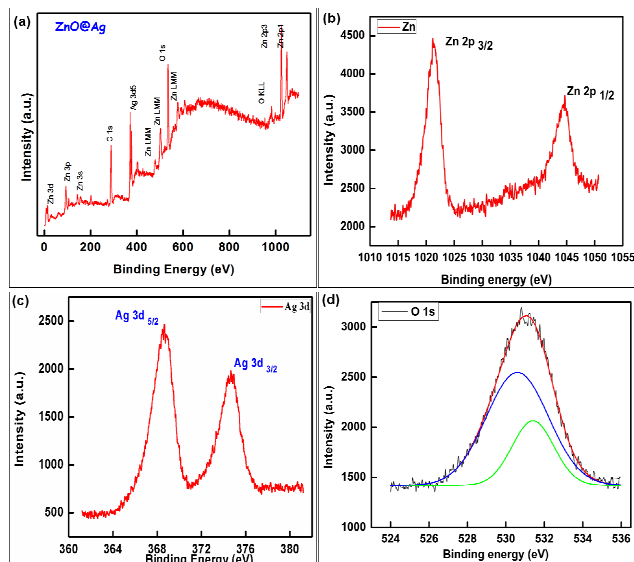


Fig. 5. XPS Spectrum of hybrid ZnO@Ag core-shell nanorods (a) Survey peak full spectrum (b) Zn 2p spectrum (c) Ag 3d spectrum (d) Fitted O 1s spectrum.

which match with XRD and HR-TEM results. Carbon peak is likely to originate from the chamber contamination in the XPS equipment. Figure 5b-d displays the high resolution spectrum of Zn, Ag and O species respectively. The peaks appearing in Figure 4b are symmetric and centered at 1021.25 and 1044.65 eV which are attributed to the Zn 2p<sub>3/2</sub> and Zn 2p<sub>1/2</sub>. Because of the strong spin-orbital coupling, the Zn 2p peak splits into Zn 2p<sub>3/2</sub> and Zn 2p<sub>1/2</sub>. Origin of the splitting is because of the charge transfer process between Zn<sup>2+</sup> and O<sup>2-</sup> caused by vacancies.<sup>39</sup> This confirms the Zn presence in the Zn<sup>2+</sup> state on the sample surface. From Figure 4c, we can find that the binding energies for Ag 3d<sub>5/2</sub> and Ag 3d<sub>3/2</sub> matches with standard peaks for Ag (Ag 3d<sub>5/2</sub> (368.2eV); Ag 3d<sub>3/2</sub> (374.2eV))<sup>40</sup> with an appreciable shift of 0.3eV. This phenomenal shift attributes to the interaction of ZnO nanorods with Ag. Also differences in the work functions of Ag (4.26eV) and ZnO (5.3eV) make the electron transfer from ZnO to Ag through the interfacial junctions during seed mediated growth.<sup>33</sup> The higher electronegative value of Ag compared to Zn initiates the electron transfer process from Zn to Ag, thus to confirm the chemical bonding between them. During the growth of Ag nanoclusters over the ZnO nanorods, fine-tuning of Fermi level occurs.<sup>19</sup> Table S2 (See Supporting Information) summarizes the binding energy values for Zn2p, Ag3d and Os1 and its corresponding *fwhm* values.<sup>41</sup> It is noticed that small appreciable shifts in binding energy values with the normal *fwhm* values of the elements reveal the presence of element in their high defective states. In Figure 4d the O1s profile asymmetric nature is observed with peak positioned at 530.60 and 531.4 eV. This corresponds to the lattice oxygen of ZnO and Oxygen related defects of Zn<sup>2+</sup>. Further, the formation of hybrid ZnO@Ag core-shell nanorods were spectroscopically confirmed using FT-IR spectroscopy (See supporting information, Figure S4), and thermal stability of the material was monitored using Thermo Gravimetric Analysis (See supporting information, Figure S5).



## Photocatalytic studies

Evaluation of photocatalytic activity was carried out for ZnO nanorods and hybrid ZnO@Ag core-shell nanorods initially using Rhodamine 6G (R6G) as the standard dye and further evaluation was performed for two industrial textile dyes namely, Congo red and Amido black10B by both UV irradiation ( $\lambda = 360$  nm) and solar irradiation (AM = 1.5G). Photocatalytic activity of the material was studied by monitoring the degradation of standard R6G dye in aqueous medium. Optical spectra obtained for the R6G dye during the photocatalytic degradation process (UV and solar irradiation) as a function of time are shown in Figure 6 and Figure S6 (See supporting information) for the ZnO@Ag and ZnO nanorods respectively. Quantitative photocatalytic process could be monitored by studying the relative concentration changes of R6G dye during photocatalysis; by monitoring characteristic absorbance of R6G at 525 nm. Photocatalytic degradation pattern observed by hybrid ZnO@Ag core-shell nanorods (Figure 6a, b) for UV-irradiation and solar irradiation was found to pursue the similar pathway. Hybrid ZnO@Ag core-shell nanorods showed much faster degradation with 28 minutes photolysis time for the complete degradation whereas, for ZnO nanorods only partial decomposition was observed during this period as shown in Figure 7. By plotting  $\ln(C/C_0)$  as a function of time, rate constant,  $k$  was obtained (See Supporting Information, Figure S7).<sup>42</sup> Rate constant for R6G without the photocatalyst was found to be negligible under UV irradiation ( $4.3 \times 10^{-4} \text{ min}^{-1}$ ) compared to ZnO and hybrid ZnO@Ag core-shell nanorods (vide Table S3). It was observed that hybrid ZnO@Ag nanorods exhibited higher photocatalytic activity as compared to the ZnO nanorods, since Ag nanoclusters on the hybrid ZnO@Ag core-shell facilitate the interfacial charge transfer process thus utilizing the CB electrons and acting as a reservoir for the free electrons.<sup>32</sup> Here, it is evident that the photocatalytic activity increases significantly for the hybrid ZnO@Ag core-shell nanorods as compared to the bare ZnO nanorods, which proves the positive role of Ag nanoclusters in the photodegradation process. Photolysis time for 50% degradation of R6G dye using ZnO was 9 minutes, whereas, for hybrid ZnO@Ag photolysis time was decreased to 4 minutes. This enhanced photodegradation effect observed by the hybrid materials compared to the ZnO nanorods alone is endorsed due to the synergetic effect and charge transfer kinetic process done by the addition of Ag nanoclusters on the surface of the ZnO nanorods.<sup>34</sup> Moreover, the higher crystalline nature with smaller size of Ag nanoclusters of hybrid ZnO@Ag core-shell nanorods plays an important role in the enhanced photocatalytic effect. From the photocatalysis results, it was observed that photo degradation of R6G occurs through oxidative pathway by photogenerated holes leading to an irreversible permanent mineralization process.<sup>43,44</sup> The major end products after oxidative degradation of R6G are  $\text{CO}_2$ ,  $\text{H}_2\text{O}$ ,  $\text{NO}_3^-$  and  $\text{NH}_4^+$  and as shown in Figure 6c.

In general, photocatalytic process of hybrid ZnO@Ag based materials is a complex process and could be explained in detail using the band structure. Surface anchoring of noble metals on the surface of metal-oxides influence the interfacial charge transfer processes as depicted in Figure 8. As the Fermi energy level of ZnO is higher than Ag, it will direct to migration of  $e^-$

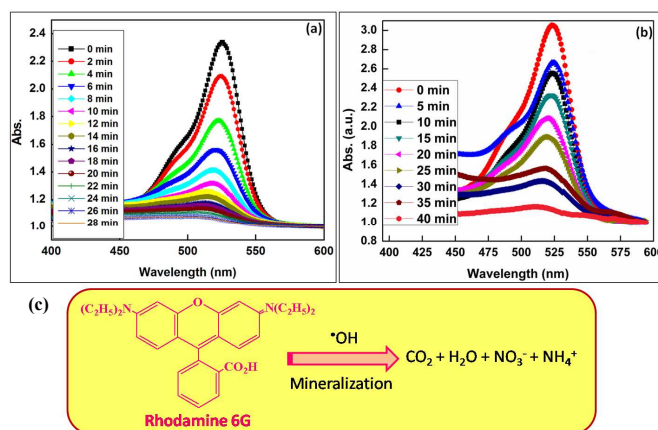


**Fig. 6.** Optical absorbance spectra monitoring the photocatalytic degradation process of R6G dye using ZnO@Ag core-shell nanorods (a) UV-irradiation, (b) Solar-irradiation and (c) oxidative degradation pathway of R6G by ZnO@Ag core-shell nanorods.

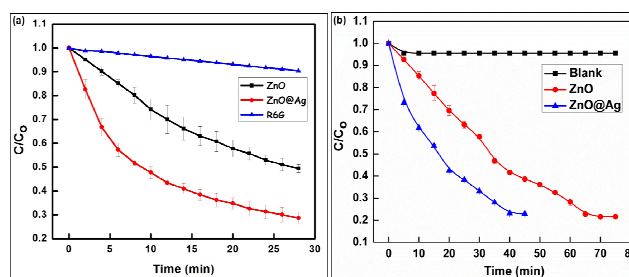


**Fig. 7.** Change in R6G concentration ( $C$ ) relative to the initial concentration ( $C_0$ ) during the photocatalytic degradation using ZnO, ZnO@Ag and blank as a function of time under (a) UV-Irradiation and (b) Solar-Irradiation.

from ZnO to conduction band of Ag in order to achieve Fermi energy level equilibrium ( $E_f$ ) (Figure 8a). Irradiation of ZnO@Ag core-shell nanorods with energy equal to or higher (UV and solar irradiation) than the band gap energy results in the promotion of an electron ( $e^-$ ) from the valance band (VB) to the conduction band (CB) leaving a hole ( $h^+_{vb}$ ) in the valance band. The  $e^-_{cb}$  (photoelectrons) can be transferred from ZnO to Ag driven by the potential energy. Ag clusters, acting as electron sink, thereby reducing the recombination of photoinduced electrons and holes but also prolong the lifetime of photogenerated pairs and move them towards the surface of the particles. As moved towards the surface, electrons ( $e^-_{cb}$ ) will be scavenged by the adsorbed oxygen molecule ( $\text{O}_2$ ) and results in the formation of superoxide anion radical ( $\text{O}_2^-$ ). Whereas, holes ( $h^+_{vb}$ ) generated at valence band will react with the surface bound hydroxyl groups ( $\text{OH}^-$ ) and water molecules to form hydroxyl and hydroperoxyl radicals respectively ( $\text{OH}$  and  $\text{HO}_2$ ) as shown in Figure 8b.

In order to achieve enhanced photocatalysis, uniform surface anchoring of Ag nanoclusters is desirable, due to the active role of Ag and ZnO nanorods in the dye degradation process though electron transfer process. Hence, an optimal loading of Ag nanoclusters is required. Drastic increase in concentration of Ag nanoclusters on ZnO nanorod surface induce aggregation of Ag clusters into larger particles, which in turn decreases the photocatalysis as confirmed from XRD studies. In the hybrid ZnO@Ag core-shell nanorods Fermi level of Ag is lower than

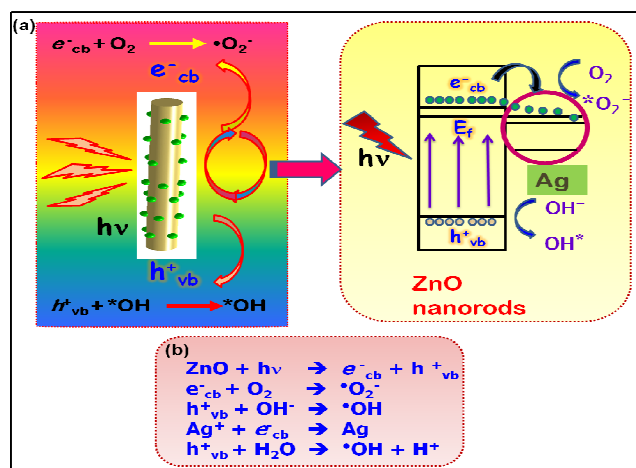


**Fig.8.** (a) Mechanism of Photocatalysis by hybrid ZnO@Ag core-shell nanorods, where Ag acts as sink for photogenerated electrons and (b) corresponding electron transfer processes during photocatalysis.

ZnO nanorods (upon UV or solar irradiation) and hence photo-excited electrons can be transferred from ZnO nanorods to Ag nanoclusters by the above driven potential energy due to the plasmonic effect.<sup>45,46</sup> Ag nanoclusters acts as electron sink as it generally reduces the recombination process of photoinduced  $e^-$  and  $h^+$ . It also increases the life time of thus generated  $e^-$  and  $h^+$  pairs. The electron transfer process will take place until the overall Fermi level of hybrid ZnO@Ag nanorods get shifted to negative potential and equilibrates with ZnO nanorods.<sup>46</sup> After attaining the equilibrium state, Ag nanoclusters discharges the captured  $e^-$  into the solution, which in-turn reacts with the dissolved oxygen to form the superoxide's and hydroxyl radicals. These highly reactive species ( $\cdot OH$ ,  $\cdot O_2^-$ ) will degrade the dye molecule into simpler molecules. Dye regeneration process is not possible in this system, as no back electron transfer process have been observed between the excited dye radical (R6G dye $^+$ ) and  $e^-$  (ZnO). This regeneration process was suppressed by Ag nanoclusters which act as a sink for the CB free electrons ( $e^-_{cb}$ ) and thus generating more VB holes ( $h^+_{vb}$ ), which in turn promoted enhanced photocatalytic process. Thus, Ag nanoclusters loaded onto the surface of ZnO nanorods facilitates the interfacial charge transfer process by utilizing the CB electrons, proving the significance of Ag in the photocatalytic process. Effect of varied pH conditions on the activity of ZnO@Ag hybrid core-shell nanorods was also monitored which showed varied % of degradation. Materials responded both in acidic and alkaline medium and maximum % of degradation was observed in alkaline medium (See supporting information, Figure S8). Similarly, photocatalytic degradation of R6G dye was carried out using hybrid ZnO@Ag core-shell nanorods under dark condition (Supporting information, Figure S9). No major changes were observed for the characteristic peak monitored at 525 nm for 30 minutes clearly emphasising the degradation phenomenon was a photo-dependent process.

In order to investigate the efficiency of the ZnO@Ag core-shell nanorods in industrial textile dye degradation, commercial dyes widely used in dyeing industries, such as, Congo red and Amido-black 10B were selected and their photodegradation

studies were performed under both UV irradiation and solar irradiation. Similar experimental conditions applied for standard R6G were adopted for these commercial dyes also. Figure 9(a,b) shows the degradation profiles of Congo red dye under UV and solar irradiations conditions. Oxidative pathway (Figure 9c) followed by Congo red dye was due to the photo generated holes, accordingly leading to the mineralization process and results in the production of  $CO_2$ ,  $H_2O$ ,  $NO_3^-$ ,  $NH_4^+$  and  $SO_4^{2-}$ .<sup>47</sup> From Figure S10, (See Supporting Information) it is understood that the catalytic activity increases noticeably for ZnO@Ag core-shell nanorods than ZnO nanorods, proving the effect of Ag nanoclusters. It is observed that time corresponding to 50% dye degradation is 12 minutes for hybrid ZnO@Ag nanorods when compared to ZnO nanorods which is 22 min for UV irradiated samples, whereas for solar irradiated samples similar pattern was observed with faster degradation rate for hybrid ZnO@Ag core-shell nanorods than ZnO nanorods (See Figure S11, Supporting Information), indicating the positive role of Ag plasmonic effect in both UV irradiated and solar irradiated samples.

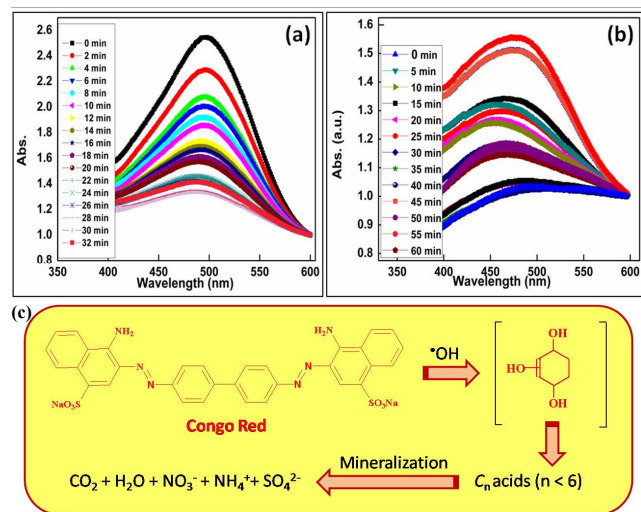


**Fig.9.** Optical absorbance spectra monitoring the photocatalytic degradation process of Congo Red using ZnO@Ag core-shell nanorods under (a) UV-irradiation, (b) Solar-irradiation and (c) oxidative degradation pathway of Congo Red by ZnO@Ag core-shell nanorods.

Similar degradation pattern was observed for Amido black 10B dye and higher catalytic activity was observed for hybrid ZnO@Ag nanorods compared to ZnO nanorods. Figure 10a and 10b depicts optical absorbance spectra showing dye degradation profile of Amido Black 10B under UV irradiated and solar irradiated conditions respectively. The degradation process observed by Amido Black 10B dye suggests, the photogenerated holes were responsible for oxidative pathway followed by irreversible permanent mineralisation process.<sup>48</sup> Similarly, Figure S12 shows the optical absorbance spectra for ZnO nanorods under UV and solar irradiated conditions. As evident from Figure S13a (See Supporting Information) the time taken for 50 % degradation of dye for ZnO nanorods was 26 minutes but for hybrid ZnO@Ag core-shell nanorods it was observed to be 12 minutes under UV irradiation, owing to the enhanced photocatalytic effect due to its hybrid core-shell nanostructure. Similarly, for solar irradiated samples degradation pattern followed by hybrid ZnO@Ag was faster as compared to ZnO

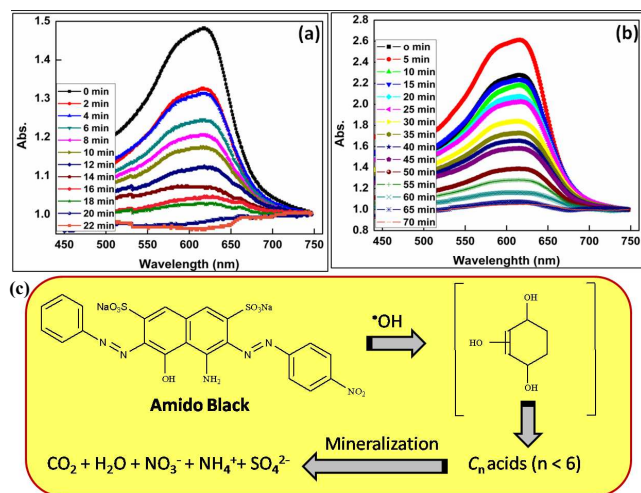


**Fig. 10.** Optical absorbance spectra monitoring the photocatalytic degradation process of Amido Black 10B using ZnO@Ag core-shell nanorods (a) under UV-irradiation, (b) under solar-irradiation and (c) oxidative degradation pathway of Amido Black 10B.

nanorods (vide Figure S13b, Supporting Information), indicating the positive role of plasmonic effect of Ag nanoclusters. Degradation studies were carried for textile effluent samples collected from a textile industry located in Thirupur, India, whose pH was neutralized to 7 from 9. Higher catalytic activity was observed for hybrid ZnO@Ag nanorods compared to ZnO nanorods for the degradation of effluent. Figure 11 and S14 depicts optical absorbance spectra showing dye degradation profile for textile effluent using ZnO@Ag core-shell nanorods and ZnO nanorods respectively. The time taken for 50% degradation of the effluent for ZnO nanorods (See Supporting Information, Figure S15) was 24 minutes but for hybrid ZnO@Ag core-shell nanorods it was observed to be 8 minutes owing to the enhanced photocatalytic effect due to the hybrid core-shell nanostructure for UV irradiated samples.

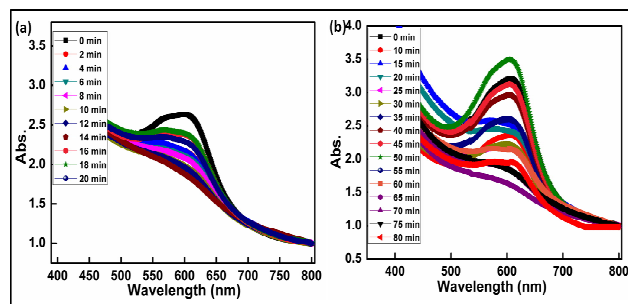


**Fig. 11.** Optical absorbance spectra monitoring the photocatalytic degradation process of Textile effluent using ZnO@Ag core-shell nanorods under (a) UV-irradiation and (b) Solar-irradiation.

For all the dyes used in this investigation, hybrid ZnO@Ag core-shell nanorods showed an enhanced photocatalytic activity with a rate constant ( $k$ ), compared to ZnO nanorods (See supporting information, Table S3). The phenomenal increase in rate constant value of hybrid nanomaterials can be attributed to the plasmonic enhancement due to the presence of Ag nanoclusters. Also, nanoclusters with very small size and large

surface area provide more active sites for charge carriers to react with surface absorbed molecules to form radical species. Degradation efficiency of hybrid ZnO@Ag core-shell nanorods showed maximum degradation compared to ZnO (vide Table 1) for both UV irradiated and solar irradiated indicating the enhanced effect of Ag nanoclusters due to plasmonic effect. This proves the hybrid ZnO@Ag core-shell nanorods can be used as an effective photocatalytic material and can be the alternative for conventional TiO<sub>2</sub> based systems during textile effluent treatment processes.

**Table 1** Comparison of % degradation efficiency and rate constant of R6G dye with Industrial dyes and textile effluent by ZnO nanorods and hybrid ZnO@Ag core-shell nanorods.

Sample	Table 1. Comparison of % degradation efficiency and rate constant of R6G dye with Industrial dye by ZnO nanorods and hybrid ZnO@Ag core-shell nanorods.							
	Degradation efficiency R6G dye		Degradation efficiency Congo Red		Degradation efficiency Amido black10B		Degradation efficiency textile effluent	
	UV (%)	Solar (%)	UV (%)	Solar (%)	UV (%)	Solar (%)	UV (%)	Solar (%)
Blank	0.01	0.01	0.01	0.01	0.01	0.01	0.01	0.01
ZnO-NR	67	58	65	61	60	66	68	64
ZnO@Ag	98	89	97	87	97	90	92	94

## CONCLUSIONS

To summarize, two-step simple facile process based on a combined hydrothermal and seed mediated growth was used to develop hybrid ZnO@Ag core-shell nanorods, constituting Ag nanoclusters on the surface of ZnO nanorods. As a seed mediated growth method, controlled deposition of Ag nanoclusters onto ZnO surface had been achieved as evident from the XRD studies. Core-shell nanorods constituents of ZnO@Ag were morphologically and structurally confirmed by SEM, TEM and XPS studies. Presence of characteristic SPR band in the UV-visible spectra of hybrid core-shell nanorods along with excitonic peak of ZnO nanorods clearly indicates the formation of hybrid nanostructured materials. It was observed that [111] facets Ag growing over ZnO nanorods ([001] facets) in a morphologically controlled manner. UV emission observed in PL spectra of hybrid core-shell nanorods was found to be dramatically quenched, indicating the suppression of electron-hole recombination process. Hybrid ZnO@Ag core-shell nanorods was found to exhibit excellent photocatalytic properties towards degradation of R6G, Congo Red and Amino Black10B dyes owing to the plasmonic effects of Ag nanoclusters on ZnO nanorods surface under UV and solar irradiations. The ZnO@Ag core-shell nanorods also showed good dye degradation properties for real time industrial textile effluent samples. The photocatalytic process was found to be enhanced for the hybrid ZnO@Ag core-shell nanorods than ZnO nanorods due to the interfacial charge transfer process. Plasmonic Ag nanoclusters located on the surface of ZnO nanorods act as electron sinks, inducing the formation of holes in valance band and electrons in conduction band respectively, which in-turn enhances the photocatalytic efficiency. The results prove that hybrid ZnO@Ag core-shell nanorods are promising material with excellent photocatalytic

properties owing to the plasmonic effect and can be effectively used for industrial textile dye degradation processes during effluent treatments.

## ACKNOWLEDGEMENTS

The authors wish to acknowledge the facilities and support provided by the management, PSG Sons and Charities, Coimbatore and Materials Science Group, IGCAR, Kalpakkam.

## AUTHOR INFORMATION

<sup>a</sup> Nanotech Research Facility, PSG Institute of Advanced Studies, Coimbatore - 641 004, INDIA. Fax: +91-42-2257-3833; Tel: +91-422 4344000, Extn (4193); E-mail: [bijuja123@yahoo.co.in](mailto:bijuja123@yahoo.co.in)

<sup>b</sup> Indira Gandhi Center for Atomic Research, Kalpakkam - 603102, INDIA. Fax: +91-44-27480081; Tel: +91-44-27480500, Extn (22507)

† Electronic Supplementary Information (ESI) available: FT-IR, TGA, FE-SEM studies and XRD of hybrid ZnO@Ag core-shell nanorods, XRD studies of ZnO nanorods, photocatalytic degradation profiles of R6G, AmidoBlack10B and Congo red using ZnO nanorods and pH dependent photocatalytic degradation of ZnO@Ag core-shell nanorods. See DOI: 10.1039/b000000x/

## REFERENCES

- I.K. Konstantinou and T.A. Albanis, *Appl Catal B: Environ*, 2004, 49, 1–14.
- S.Ameen, M.S. Akhtar, Y.S. Kim and H.S. Shin, *Appl Catal B: Environ*, 2011, 103, 136–142.
- V. Meshko, L. Markovska, M. Mincheva and A.E. Rodrigues, *Wat. Res.* 2001, 35, 3357–3366.
- S.P. Sampat Rao and M.S. Vijay, *Environ. Sci. Technol.*, 1988, 22, 1160–1165.
- T. M. Alan, V. Alex and F. Samuel, *Environ. Sci. Technol.*, 1989, 23, 403–406.
- L.T. Tracy and T.Y. John, *Chem. Rev.*, 2006, 106, 4428–4453.
- K. Vinodgopal, D.E. Wynkoop and P.V. Kamat, *Chemtech.*, 1996, 4, 18.
- P.V. Kamat, *Chem. Rev.*, 1993, 93, 267–300.
- Y. Zheng, C. Chen, Y. Zhan, X. Lin, Q. Zheng, K. Wei, J. Zhu and Y. Zhu, *Inorg. Chem.*, 2007, 46 (16) 6675–6682.
- D. Pingfan, S. Lixin, X. Jie and C. Houbao, *J. Mater. Sci.*, 2013, 48, 8386–8392.
- Z. Xiang, T. Velmurugan, S.G. Mhaisalkar and R. Seeram, *Nanoscale*, 2012, 4, 1707–1716.
- N. Serpone, D. Lawless and R. Khairutdinov, *J. Phys. Chem.*, 1995, 99, 16646.
- U. Nayane, L. Myeongsoon, K. Junhyung, L. Dongil, *ACS Appl. Mater. Interfaces*, 2011, 3, 4531–4538.
- M. A. Mahmoud, W. Qian and M.A. El-Sayed, *Nano Lett.*, 2011, 11, 3285–3289.
- D.B. Ingram and S. Linic, *J. Am. Chem. Soc.*, 2011, 133, 5202–5205.
- C.H. Chen, S. J. Chang, S. P. Chang, M.J. Li, I.C. Chen, T.J. Hsueh and C.L. Hsu, *Appl. Phys. Lett.*, 2009, 95, 223101.
- C.H. Ye, Y. Bando, G.Z. Shen and D. Golberg, *J. Phys. Chem. B* 2006, 110, 15146–15151.
- L. Rui, W. Ping, W. Xuefei, Y. Huogen and Y. Jianguo, *J. Phys. Chem. C*, 2012, 116, 17721–17728.
- M.R. Jones, K.D. Osberg, R.J. Macfarlane, M.R. Langille and C. Mirkin, *Chem. Rev.* 2011, 111, 3736–3827.
- L. Myeongsoon, A. Piyadarsha, K. Junhyung and L. Dongil, *J. Phys. Chem. C*, 2010, 114, 18366–18371.
- Y.H. Zheng, C.Q. Chen, Y.Y. Zhan, X.Y. Lin, Q. Zheng, K.M. Wei and J.F. Zhu, *J. Phys. Chem. C*, 2008, 112, 10773–10777.
- N. Yong-hong, W. Xian-Wen, H. Jian-ming and Y. Yin, *Mater. Sci. Eng. B Adv.*, 2005, 121, 42–47.
- L. Peng, W. Zhe, W. Tong, P. Qing and L. Yadong, *J. Am. Chem. Soc.*, 2011, 133, 5660–5663.
- Y.C. Lu, Y. H. Lin, D.J. Wang, L.L. Wang, T.F. Xie and T.F. Jiang, *J. Phys. D: Appl. Phys.*, 2011, 44, 315502.
- T. Linnert, P. Mulvaney, A. Henglein and H. WeUer, *J. Am. Chem. Soc.*, 1990, 112, 4657–4664.
- P. B. Sarawade, S. M. Kim, K. D. Kim and H. T. Kim, *Journal of Industrial and Engineering Chemistry*, 2014, 20, 1830–1833.
- Z.Y. Huang, G. Mills and B. Hajek, *J. Phys. Chem.*, 1993, 97, 11542.
- M.J. Hostetler, J.E. Wingate, C.J. Zhong, J.E. Harris, R.W. Vachet, M.R. Clark, J.D. Londono, S.J. Green, J.J. Stokes, G.D. Wignall, G.L. Glish, M.D. Porter, N.D. Evans and W.R. Murray, *Langmuir*, 1998, 14, 17–30.
- T.J. Sun, J.S. Qiu and C.H. Liang, *J. Phys. Chem. C*, 2008, 112 (3), 715–721.
- S.A. Studenikin, N. Golego and M. Cocivera, *J. Appl. Phys.*, 1998, 84, 2287.
- K. Vanheusden, C.H. Seager, W.L. Warren, D.R. Tallant and J.A. Voigt, *Appl. Phys. Lett.*, 1996, 68, 403–406.
- L. Jaeil, S.S. Hyeong, L. Myeongsoon, K.S. Jae and L. Dongil, *J. Phys. Chem. Lett.*, 2011, 2, 2840–2845.
- V. Subramanian, E.E. Wolf and P.V. Kamat, *J. Phys. Chem. B*, 2003, 107, 7479–7485.
- H.R. Liu, G.X. Shao, J.F. Zhao, Z.X. Zhang, Y. Zhang, J. Liang, X. G. Liu, H. S. Jia, B. S. Xu, *J. Phys. Chem. C*, 2012, 116, 16182–16190.
- H. Xiangyun, D. Jiangnan, Y. Chenhui, W. Zhihao, C. Changqing, G. Yihua, *Appl. Surf. Sci.*, 2010, 256, 4682–4686.
- CRC Handbook of Chemistry and Physics, 65th ed.; CRC: BocaRaton, FL, CRC/Taylor & Francis, 2006.
- Z. Rui, G. Y. Peng, W. Ning and G. Lin, *Solid State Sci.*, 2009, 11, 865–869, 27.
- W. Sun, G. Chen and L. Zheng, *Scripta Materialia*, 2008, 59, 1031–1034.
- Y.Y. Tay, S. Li, C.Q. Sun and P. Chen, *Appl. Phys. Lett.*, 2006, 88, 173118–173111.
- J.F. Moulder, W.F. Stickle, P.E. Sobol and K.D. Bomben, *Handbook of X-ray Photoelectron Spectroscopy*; Perkin-Elmer: Eden Prairie, MN, 1992.
- K.S. Ranjan, K. Ganguly, T. Mishra, M. Mishra, R.S. Ningthoujam, S.K. Roy and L.C. Pathak, *J. Colloid Interf. Sci.*, 2012, 366, 8–15.
- J. Zeng, M. Xin, K.W. Li, H. Wang, H. Yan and W. Zhang, *J. Phys. Chem. C*, 2008, 112, 4159–4167.
- I.K. Konstantinou and T.A. Albanis, *Appl. Catal., B* 2004, 49, 1–14.
- T. S. Natarajan, M. Thomas, K. Natarajan, H. C. Bajaj and R. J. Tayade, *Chem. Eng. J.*, 2011, 169, 126–134.
- M. Jakob, H. Levanon and P.V. Kamat, *Nano Lett.*, 2003, 3, 353.
- Z. Yuanhui, Z. Lirong, Z. Yingying, L. Xingyi, L.; Z. Qi and W. Kemei, *Inorg. Chem.*, 2007, 46, 17, 6980–7986.
- T. S. Natarajan, K. Natarajan, H. C. Bajaj and R. J. Tayade, *Ind Eng Chem. Res.* 2011, 50, 7753–7762.
- A. V. Salker and S. D. Gokakakar, *Int. J. Phys. Sci.*, 2005, 4(6), 377–384.